The effect of carrier gas pressure and wall heating on the operation of the thermal diffusion cloud chamber

Frank T. Ferguson[a]
Department of Chemistry, Catholic University of America, Washington, DC 20064

Richard H. Heist
Department of Chemical Engineering, Manhattan College, Riverdale, New York 10471-4098

Joseph A. Nuth III
Code 691, NASA-Goddard Space Flight Center, Greenbelt, Maryland 20771

Experimental observations indicate that the nucleation behavior within the thermal diffusion cloud chamber (TDCC) changes with increasing carrier gas pressure and applied sidewall heating, even though such an effect is not predicted by typical nucleation theories and it is not seen in typical expansion-based nucleation studies. In this work we present a model of the chamber which shows that both of these effects are likely due to buoyancy-induced convection within the TDCC. As the chamber pressure is increased, the calculated critical supersaturation within the chamber decreases. Results from a simple model of the chamber wall heating are also presented. Previously, it was argued that unheated chamber walls result in a significant, radial concentration gradient which lowers the vapor concentration and condensation flux within the chamber center. In contrast, we show that this reduction is due primarily to a convective flow induced by the sidewall concentration gradient. The model has been applied to recent experimental data for *n*-pentanol. Results indicate that, with respect to buoyancy-induced convection, the typical 1D model should be regarded as an upper limit to the maximum attainable supersaturation within the chamber. © *2001 American Institute of Physics.* [DOI: 10.1063/1.1409956]

I. INTROUCTION

For some time now there has been increasing emphasis on understanding the range of stable operation of the thermal diffusion cloud chamber (TDCC). This closer view of the chamber has been prompted by the fact that experimental TDCC results are dependent upon both the type and the amount of background, carrier gas.[1–3] This result is somewhat disturbing since such a carrier gas effect is neither predicted by the typical Classical Nucleation Theory (CNT) equations nor has it been observed in expansion-based nucleation studies.[4]

There have been several theoretical treatments of the nucleation process offered to help explain this pressure effect. Oxtoby and Laaksonen used the Nucleation Theorem to examine the effect of carrier gas pressure on nucleation.[5] Their results were similar to those of Ford that showed that the predicted theoretical magnitude of the carrier gas effect was much smaller than the experimentally observed results.[6] Kaschiev examined the carrier gas effect and its influence on the dissipation of the heat of condensation.[7] Depending upon the system, he found that the carrier gas could either stimulate or inhibit nucleation, but again the predicted magnitude of this change was less than is observed. Oh and Zeng have recently performed a Monte Carlo study of water nucleation in nitrogen and found that the barrier height to nucleation increases with pressure at 240 K, but found little change at 298 K.[8] Itkin has presented a model of nucleation in a diffusion cloud chamber which predicts a pressure effect arising from different rates of transport of condensing molecules to the growing cluster surface.[9] Kane *et al.* have argued that the observed change in condensation flux with pressure may in fact be due to a change in droplet growth and motion.[10] In certain regimes, droplets may not grow to a sufficient size to be detected by the counting system, therefore resulting in an under-representation of the actual condensation flux.

Other explanations for the observed pressure effect have focused on the actual operation of the chamber and calculation of the chamber conditions. Fisk *et al.* examined the possibility of nonideal pressure effects, but again arrived at the conclusion that the predicted magnitude of the effects were far lower than experimental observations.[11] Anisimov *et al.*[12] reexamined the equations for the static TDCC in detail and compared their results with *n*-pentanol data taken by Rudek *et al.*[13] Their newly computed supersaturation values were significantly lower for all isotherms. Ferguson and Nuth used a numerical model of the TDCC to show that buoyant convection could result in a reduction of the maximum supersaturation by several percent depending upon a variety of chamber conditions.[14] Schaeffer *et al.* performed a similar analysis, but with higher molecular weight gases.[15] Their results indicated that the TDCC behaves like a classical Rayleigh–Bénard cell, and when conditions exceed a critical value, vigorous convection can occur within the chamber.

The goal of this work is to extend previous modeling of the TDCC with emphasis on studying the effect of total pres-

[a]Electronic mail: ferguson@cua.edu

10829   © 2001 American Institute of Physics

sure on the TDCC operation. In addition to total pressure, it has been observed that the chamber flux is dependent upon the amount of heat applied to the chamber walls. In this paper we will also examine this related phenomena. Finally we reexamine the calculation of recent TDCC data for *n*-pentanol taken by two different experimental groups.

II. MODELING OF THE TDCC

A. Governing equations

The equations used to describe the TDCC are essentially the same to those given earlier in Ref. 14. The only differences in this case are that the Soret and Dufour effects have been included as well as the species interdiffusion term.

The total mass flux, $\mathbf{j_A}$, of the vapor, A, with respect to the mass average velocity within the chamber is assumed to be made up of two components: an ordinary concentration-induced diffusive flux, $\mathbf{j_A^{(x)}}$, and a flux induced by the temperature gradient (Soret Effect), $\mathbf{j_A^{(T)}}$.[16] Therefore,

$$\mathbf{j_A} = \mathbf{j_A^{(x)}} + \mathbf{j_A^{(T)}}. \tag{1}$$

In terms of the concentration and temperature gradients, these individual fluxes are, respectively,

$$\mathbf{j_A} = [-\rho D_{AB} \nabla w_A] + [-\rho D_{AB} \alpha_T w_A (1 - w_A) \nabla \ln T], \tag{2}$$

where ρ is the total density, D_{AB}, the binary diffusion coefficient, w_A, the mass fraction of component, A, α_T, the thermal diffusion ratio, and T the temperature.

Similarly, the total energy flux, $\mathbf{q}$ with respect to the mass average velocity of the system, $\mathbf{u}$, is made up of three components: the typical conduction term, $\mathbf{q^{(c)}}$, a species interdiffusion term, $\mathbf{q^{(d)}}$, and the reciprocal to the Soret effect, the concentration-induced Dufour energy flux, $\mathbf{q^{(x)}}$:[16]

$$\mathbf{q} = \mathbf{q^{(c)}} + \mathbf{q^{(d)}} + \mathbf{q^{(x)}}. \tag{3}$$

Using the simplification for a binary system that $\mathbf{j_A} = -\mathbf{j_B}$, these three terms are given, respectively, by

$$\mathbf{q} = [-k\nabla T] + [(h_A - h_B)\mathbf{j_A}] + \left[\alpha_T \frac{RTM^2}{M_A M_B} \mathbf{j_A} \right], \tag{4}$$

where k is the mixture thermal conductivity, h_i the specific enthalpy of component i, R, the ideal gas constant, and M_i and M, the molecular weights of component i and the mixture, respectively.

As stated earlier, these fluxes are written with respect to the mass average velocity of the system. Therefore the velocity components are needed to calculate the energy and mass fluxes with respect to a stationary, fixed reference frame. To fully solve for the profiles within the chamber, the momentum and continuity equations coupled with an equation of state are needed. The governing equations solved in this work are:

energy equation

$$\nabla \cdot (\rho \mathbf{u} h) = -\nabla \cdot \mathbf{q}; \tag{5}$$

vapor conservation equation

$$\nabla \cdot (\rho \mathbf{u} w_A) = -\nabla \cdot \mathbf{j_A}; \tag{6}$$

continuity equation

$$\nabla \cdot (\rho \mathbf{u}) = 0; \tag{7}$$

momentum equation

$$\nabla \cdot (\rho \mathbf{u} \mathbf{u}) = -\nabla \cdot \tau + \nabla P + \rho \mathbf{g}. \tag{8}$$

In this work it is assumed that both the vapor and background gas follow the ideal gas equation of state. In Eq. (8), P is the pressure, τ the stress tensor, and $\mathbf{g}$ the gravitational level. The stress tensor components for the system are given in detail in Ref. 14. Equations (5)–(8) can be used to calculate the temperature, concentration, and flow fields within the TDCC. These equations are solved in 2D, cylindrical coordinates using finite differences and the SIMPLER method.[14,17]

B. Boundary conditions

The boundary conditions used in this work are also quite similar to those given in Ref. 14. One important change is in the normal velocity components. Previously, it had been assumed that these components were zero. As noted by Anisimov *et al.*, the specification of an insoluble background gas leads to a nonzero velocity component at the solution boundaries.[12] For example, the mass flux of the background gas, n_B, is

$$n_{B\zeta} = -\rho D_{AB} \frac{dw_A}{d\zeta} + \rho u = 0, \tag{9}$$

where ζ is the spatial component normal to the wall. Since it is assumed that the background gas is insoluble in the liquid, then it follows that the normal velocity component, u, at the wall is

$$u = \frac{D_{AB}}{1 - w_A} \frac{dw_A}{d\zeta}. \tag{10}$$

As shown by Eq. (9), this convective flow, the so-called Stefan flow, exactly balances the diffusive flux of the background gas so there is no net transport of the background gas at the boundaries. Equation (10) is used for all velocity components normal to the bounding surfaces, including the chamber sidewall.

C. Program details

The code described in this work is written in C and can run on a variety of computers. Total running times for cases depend upon grid refinement and convergence criteria. A reasonable description of the chamber can be obtained in approximately 10 min on a typical PC (e.g., a Pentium III-450), with a coarse grid and strong convergence criteria; more refined grids such as the ones used to generate the results in this work take a little less than 1.5 h per case. No focused effort has been made to optimize these running times so these may be decreased in the future. Nevertheless it is clear that the code in this work takes much longer to run than the typical, 1D model of the chamber. Often the 1D model is run in conjunction with TDCC experiments to establish certain operating conditions, e.g., runs made at a constant nucleation temperature. At present, this 2D model would not be suitable for such experiments. The goal here is to use the 2D model
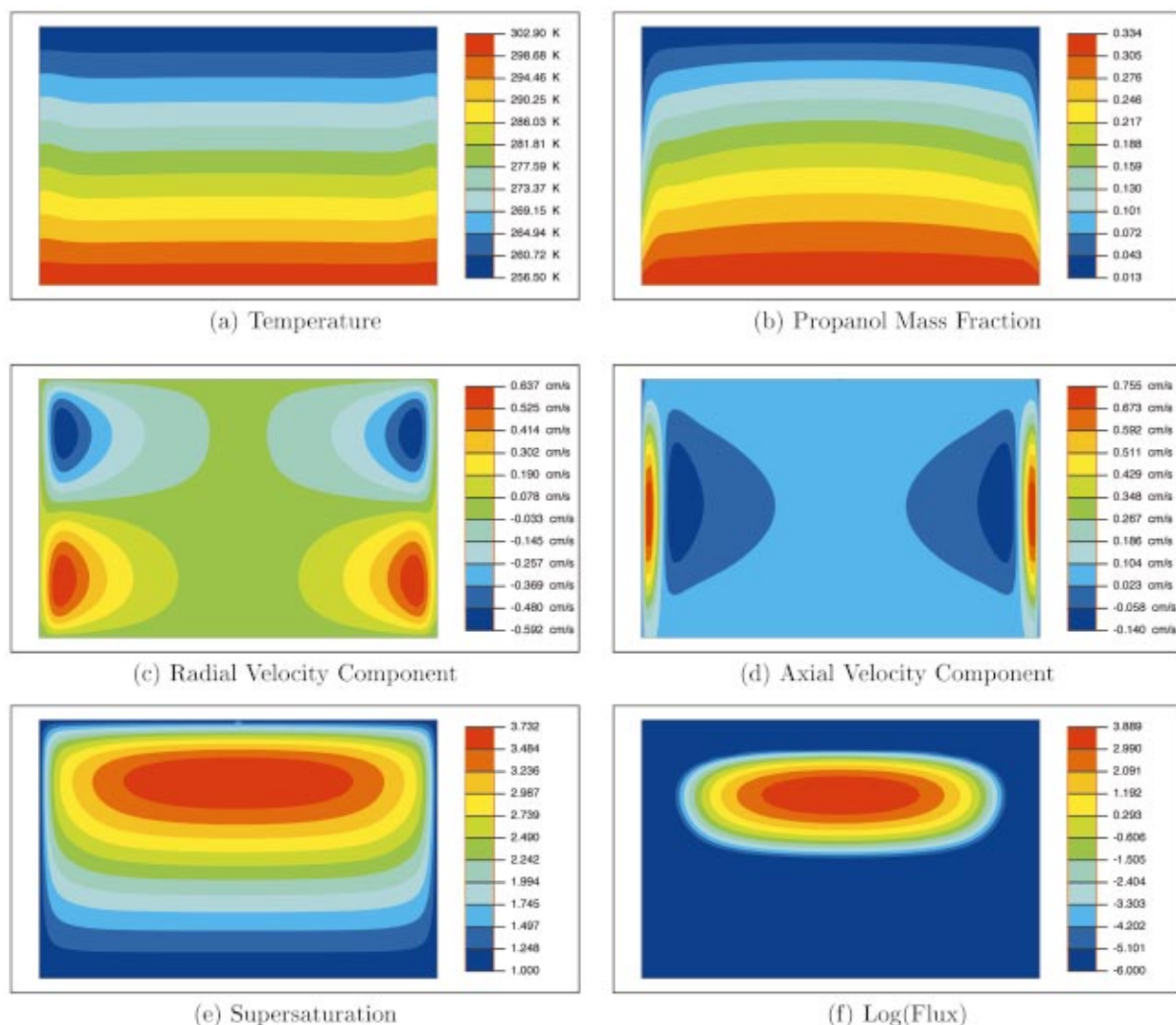
FIG. 1. (Color) Contour plots for the wet wall TDCC at 1.18 bar. Shown in the figure are the (a) temperature, (b) mass fraction of propanol, (c) radial velocity component, (d) axial velocity component, (e) propanol supersaturation, and (f) logarithm of the propanol condensation flux calculated via Classical Nucleation Theory.

to understand chamber operation and perhaps establish acceptable operating limits for the 1D description of the chamber. Since there are a variety of factors which can affect the magnitude of convection within the chamber it is reasonable to expect that other researchers working in the field may want to use this computer program to examine specific cases. Therefore, researchers interested in making such runs can obtain the computer program by contacting the authors.

III. BASELINE PROPANOL CASE

The specification of a normal velocity component in this work is a significant difference over the results given in Ref. 14. In general, the additional convective flux results in slightly higher calculated supersaturations within the chamber. Fortunately, most of the trends noted in Ref. 14 are still valid. To demonstrate this we have recalculated results for the baseline propanol test case examined in Ref. 14.

Figure 1 is a collection of contour plots of the temperature, propanol mass fraction, velocity components, supersaturation, and logarithm of the condensation flux calculated

via CNT. These results were calculated for an experimental data point taken with the High Pressure Cloud Chamber (HPCC), a version of the TDCC that has been modified to allow nucleation studies at relatively high pressures (~40 bar).[1-3] The inside diameter of this chamber is 10.38 cm and the diameter to height ratio (after accounting for the lower liquid pool) is approximately 7.5. The contour plots shown in Fig. 1 were calculated for lower and upper plate temperatures of 302.9 and 256.5 K, respectively, at a total pressure of 1.18 bar.

Both the temperature and mass fraction profiles are relatively flat—the largest disturbances are at the chamber sidewall. The large gradient in the concentration at the chamber sidewall induces the strong upward flow near the wall as shown in Fig. 1(d) and this flow is balanced by a weaker downward flow closer to the center of the chamber. This is not the only source of convective flow within the chamber. A close inspection of the axial velocity contour plot will also show that at both the upper and lower plates the axial velocities, although very small, are not nonzero. There is an over-
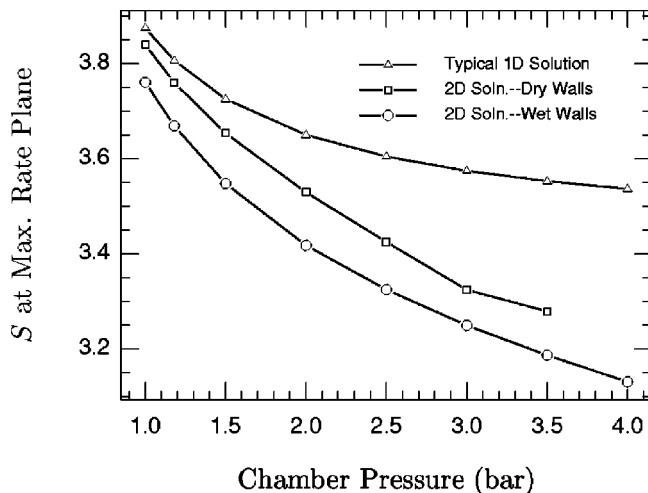
FIG. 2. The effect of pressure on the calculated critical supersaturation. Results are shown for the typical 1D model, the 2D model with dry walls and the 2D model with wet walls. For both the wet wall and dry wall cases, the subtle, single convective cell within the chamber develops into multiple cells and stronger flows as the Rayleigh–Bénard stability limit is reached in the neighborhood ~4 bar.

all, weak, upward convective flow throughout the chamber that is dictated by the boundary condition of Eq. (10). This overall convective flow was not accounted for in Ref. 14. Fortunately, this overall flow merely shifts the maximum chamber supersaturation slightly higher so that the overall trends as listed in Ref. 14 should still be valid.

IV. THE EFFECT OF PRESSURE ON THE COMPUTED SUPERSATURATION

TDCCs are typically operated in a "dry" mode in which a sufficient amount of heat is added to prevent condensation on the walls and provide a clearer view of the region of droplet formation within the chamber. In the wet mode, no heat is applied to the chamber walls and the vapor is allowed to condense on and "wet" these sidewalls. Regardless of the mode of operation, it is observed experimentally that an increase in chamber pressure results in a decrease in the chamber flux. To examine the effect of chamber pressure we have calculated the change in calculated critical supersaturation for the 1D model, typically used to describe the chamber, and the 2D model, which includes convective effects. For the 2D model, both dry and wet walls are considered. The results from these calculations are shown in Fig. 2.

All of the results shown in Fig. 2 are calculated for the propanol test case described earlier; the only change is that the pressure is now varied from 0.5 to approximately 4.0 bar. The top curve shows the variation in the calculated critical supersaturation with pressure based on the typical, 1D modeling of the chamber. In actuality, these results were calculated with the full 2D model in which the gradient of the temperature, propanol mass fraction, and axial velocity were all set to zero, in effect making the result "one-dimensional." Though in terms of computational time it is more expensive to compute the results this way, it does ensure that there are no differences due to computational grid sizes or different physical properties when we compare the

1D and 2D results. Also shown in the plot are the computed critical supersaturations for both wet and dry wall operation.

At the lowest pressures, all three models tend to give essentially the same result, but the spread between the 1D and 2D models becomes larger with increasing pressure. Above 1.5 bar, the 1D model predicts very little variation in the critical supersaturation with pressure. Both the wet and dry wall results are substantially lower than the 1D prediction. In this case the buoyancy forces induced by the wet wall boundary condition are stronger than for the dry wall one and there is a stronger depression in the critical supersaturation for this mode than for the dry at any given pressure. It should be noted that the dry wall boundary condition was computed assuming ideal heating of the walls—any differences from this profile should result in even lower calculated supersaturations.

It is important to stress how the results shown in Fig. 2 would appear in a typical experiment. If the chamber were set at a point where it was critically nucleating, and the pressure was increased, then as shown by the curves in Fig. 2, the actual critical supersaturation within the chamber is reduced. Yet, the typical 1D model would indicate that the critical supersaturation changed negligibly. In order to get the chamber critically nucleating again, the chamber conditions would have to be changed somewhat and the critical supersaturation recalculated. This newly recalculated value of the critical supersaturation can result in an "apparent" increase in the critical supersaturation with pressure.

The reduction in the dry/wet wall critical supersaturation with pressure occurs solely due to the sidewall-induced buoyancy. In the wet wall case, the flow is generated by concentration-induced changes in the density while in the dry wall case it is caused by thermally induced buoyancy. To verify that the reduction was due solely to convection, the 2D model was run with the gravitational level set to zero. These results were essentially identical to the 1D curve shown in Fig. 2. The fact that the two boundary conditions give the same result in the absence of convection is also supported by the modeling results of Bertelsmann and Heist.[18]

For both the dry and wet wall cases we note that as the pressure is increased, the Rayleigh–Bénard stability limit, as noted by Schaeffer et al. is eventually reached.[15] Above this point, the single convective cell shown in Fig. 1 develops into a multicellular feature in which the contours of the temperature and mass fraction are no longer flat. For the dry wall configuration, this occurs just under 4 bar and for the wet wall case it occurs just above this point. It should also be noted that for these conditions, the Rayleigh–Bénard stability limit occurs at a relatively low pressure. For other plate temperatures, this critical pressure may be much higher.

In regards to convection induced by sidewall buoyancy, the results shown in Fig. 2 seem to suggest that the most reliable results will be obtained at the lowest pressures. Practically, this may not be feasible since the vapor flux increases significantly at the lowest pressures and the calculated results can be very sensitive to the quantities used to compute this flux, including the measured variables (such as plate and
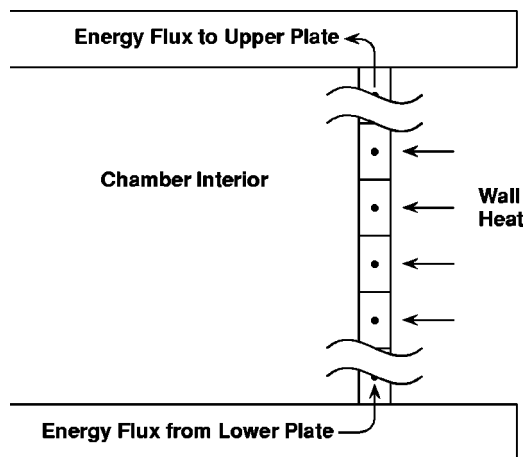
FIG. 3. Simple model of wall heating. The chamber wall is divided into a number of control volumes. Only transport due to conduction along the wall and applied heating are considered.
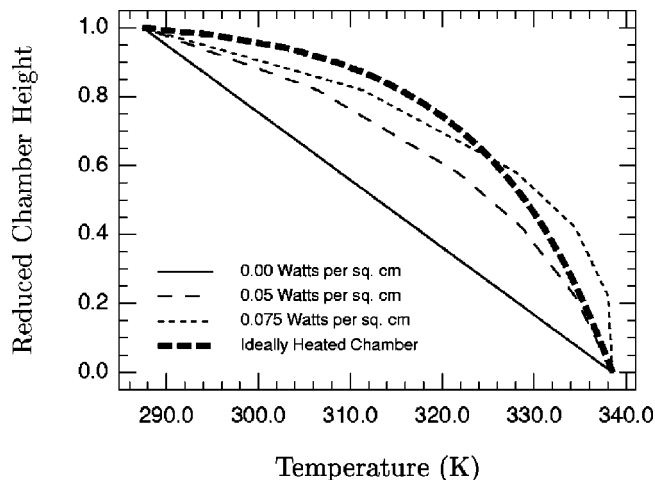

FIG. 4. Temperature variation along the chamber sidewall. Shown in the figure are the computed results for the wall temperature as a function of applied heat flux and the temperature distribution for an ideally heated wall.

liquid pool temperatures), and physical property values (e.g., equilibrium vapor pressure data).[19,20]

V. EFFECT OF WALL HEATING

It has been experimentally observed that the condensation flux can be a function of the amount of heat applied to dry the TDCC walls.[11] In this section we examine the reason for this variation by making a simple model of the wall heating.

Consider the diagram of the chamber sidewall shown in Fig. 3. Fisk *et al.* have argued that the temperatures at the top and bottom of the sidewall are fixed by the temperatures of the upper/lower plates, respectively.[11] If conduction is the dominant transport mechanism through the sidewall, then Fisk *et al.* reasoned that there will be an essentially linear temperature drop along the plate.

In this work we wish to make a simple model of the chamber wall heating. To do this we divide the chamber wall into small control volumes and include conduction along the wall and applied heat, but neglect cooling or heating to/from the ambient surroundings. The advantage of this simple model of the wall is that the calculation of the wall temperatures can be decoupled from the calculation of the flow within the chamber interior.

Consider a single control volume similar to those shown in Fig. 3. Assume that each of these volumes has a height of Δz. Then for each of these volumes the rate of energy input to the volume is given by the product of the fluxes at the boundary and the area of each volume element. The rate of energy input into each volume is given by

$$q_j[2\pi R_0 \Delta z] + \left[k \frac{dT}{dz}\bigg|_b \right][\pi(R_0^2 - R_i^2)], \tag{11}$$

where q_j is the applied energy flux from the heating wire to a control volume, j, R_0 the outside radius of the chamber, R_i the inside radius of the chamber, k the thermal conductivity of the wall. The subscript b represents the bottom face of the element.

Likewise, the rate of energy leaving each volume is just the conductive loss given by

$$\left[k \frac{dT}{dz}\bigg|_t \right][\pi R_0^2 - R_i^2)], \tag{12}$$

where t represents the top face of the control volume. Under steady conditions, an energy balance gives

$$\left[\frac{dT}{dz}\bigg|_b - \frac{dT}{dz}\bigg|_t \right] = \frac{-2R_0 \Delta z q_j}{k(R_0^2 - R_i^2)}. \tag{13}$$

By representing the temperature derivatives at the faces by finite differences we have

$$T_j = \frac{1}{2}(T_{j+1} + T_{j-1}) - \frac{2R_0(\Delta z)^2 q_j}{k(R_0^2 - R_i^2)}. \tag{14}$$

According to Eq. (14), if there is no wall heat input, then the temperature profile along the wall will be linear. For any heat input (given by a negative q_j in the coordinate system used here) the temperature at any given point along the wall will be higher than this linear profile.

The term which accounts for heating of the wall depends upon a variety of things including the chamber size, wall thickness, and thermal conductivity of the wall material. It is assumed that four heater wires are used and are equally spaced along the chamber wall. Therefore, in general the heat flux terms will be zero and only at the control volumes corresponding to these four points will there be a nonzero q_j term.

Figure 4 is a plot of the results of such a wall calculation. The results were calculated for a chamber inner radius of 14.5 cm and height of 4.2 cm corresponding to the size of Chamber II used by Rudek *et al.* in their pentanol experiments. The upper plate temperature was set at 287.44 K and the lower plate temperature was 338.53 K. The chamber wall thickness was assumed to be 0.95 cm and the thermal conductivity of the wall was then taken as that of Pyrex at 300 K.
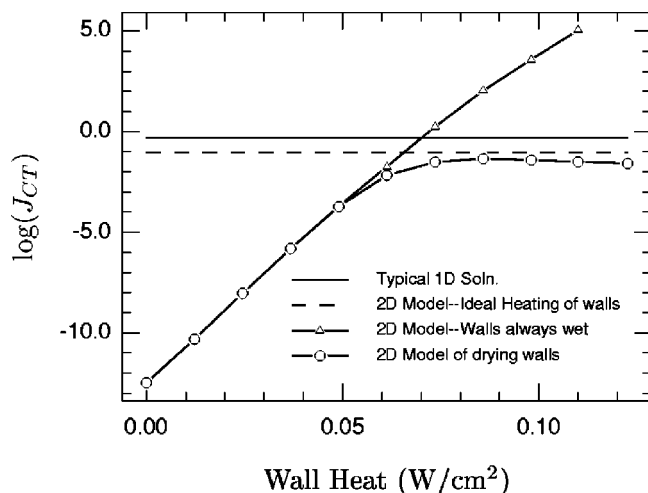
FIG. 5. Computed fluxes as a function of applied wall heat. As heat is applied to the dry wall model, the results reach a "plateau" in which the flux is relatively insensitive to the applied wall heat. The computed fluxes will always be less than the ideally heated wall case.

In actually heating the chamber, a large fraction of the energy is typically applied to the upper section. This distribution of the total dissipated power is given in Ref. 11 and these same fractions were used in computing the wall temperatures in this work.

As shown in the figure, with no wall heating there is a linear drop in temperature. As the amount of heat is increased, the temperature of the wall increases. The curves shown represent different amounts of applied power (in Watts) divided by the total sidewall surface area (in cm^2). Also shown in the figure is the temperature profile needed to produce ideal heating. For a wall heat of 0.075 W cm^{-2}, part of the temperature profile exceeds this ideal value, while the remainder falls below. Such profiles are used as the sidewall boundary condition to the model and the modeling results are given in the following section.

A. Vapor boundary condition

In the previous section, a detailed description was given for the method used to calculate the wall temperature given specific heating rates. The vapor boundary condition is equally important and a review of the method used to calculate it will be given here.

In actual operation, when the chamber wall is unheated there is transport of vapor to the wall where it wets the surface. Under this condition it is assumed that the vapor concentration is given by the equilibrium vapor pressure of the condensed liquid at the temperature of the wall at that point. At some time, as the wall is heated, the vapor flux reverses direction and the wall acts as a source for vapor rather than a sink. This is a temporary situation since eventually the source for this vapor flux, the liquid on the sidewall, will be depleted and will "dry up." At a certain temperature along the wall there is a transition from a wet wall boundary to a dry one. To simulate this effect we use a hybrid boundary condition. First we calculate the equilibrium vapor pressure at the temperature of the sidewall. If this value results in a negative gradient (i.e., a flux to the wall and hence wetting of

the wall), then the wall concentration is set to this equilibrium value. Otherwise the gradient at the wall is set to zero, since given sufficient time, such a temperature is large enough to deplete the vapor at this point.

B. Heating results

The results from the runs with the simple wall heating model are shown in Fig. 5. Shown in the plot are the calculated condensation fluxes as a function of applied wall heat (in Watts) divided by the total chamber sidewall surface area. Although the data is plotted this way to facilitate comparison with experimental data for this system taken by Rudek et al.,[13] it is important to note that the two may not quantitatively agree since the wall heating model here does not consider losses to the ambient environment or the efficiency of the energy transmission from the heater wires to the sidewall.

In Fig. 5, the expected results from the typical 1D model are shown as the solid horizontal line. The dashed horizontal line represents the calculated maximum flux within the chamber when the chamber sidewalls are ideally heated. Even in this ideal condition there is some reduction in the maximum flux due to buoyancy-induced, convective flows.

If the chamber wall is not heated, the flux within the chamber is many orders of magnitude below both horizontal lines. It has been argued by Fisk et al. that with unheated walls, the flux in the chamber is significantly lower due to a radial concentration gradient.[11] Although the flux is reduced, this is not the reason for the reduction. It occurs because the concentration gradient at the wall induces a convective cell, which diminishes the maximum supersaturation in the center of the chamber. This was verified by setting the gravitational level to zero in the model (effectively eliminating buoyant convection, yet maintaining the diffusive concentration gradient). The results were then identical to the 1D result and were not influenced by the amount of wall heat.

If by some method the chamber walls could always remain wet and never become dry, then calculations show that the condensation flux would continue to increase with wall heat as shown in the figure. If, on the other hand, the hybrid, boundary condition is used to simulate drying of the walls, then the condensation flux tends to level off and nearly reach the value of the ideal heating flux. This is quite interesting since this behavior is similar to what is experimentally observed. At a sufficient amount of wall heat, there is a "plateau" in the condensation flux. It is also interesting to note that the plateau in Fig. 5 occurs at a wall heating value that is comparable to that experimentally measured.[13] The value here is somewhat smaller, but this is to be expected since this model assumes perfect transmission of energy from the heating wires to the wall.

C. Size of the chamber

Maintaining a large aspect ratio in the TDCC is vital in maintaining fluxes within the chamber that are plane-parallel to the lower and upper plates and in minimizing wall effects. In the typical 1D modeling, the actual dimensions of the chamber are not needed to describe the system, as long as the
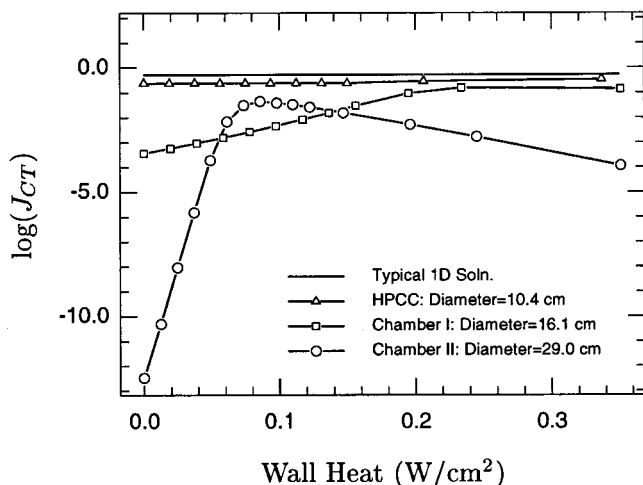
FIG. 6. Computed fluxes as a function of chamber size. As the size of the chamber is reduced, the influence of convection on the results also decreases and the behavior approaches that predicted by the typical 1D equations.

plane-parallel approximation remains valid. Previously, it was shown that this is no longer the case in terms of convection since the magnitude of the flow scales with the volume of the chamber.[13] Therefore, it is possible that two different sized chambers, operating under identical conditions and aspect ratios, may give different results due to enhanced convection in the larger chamber.

To investigate this effect we have examined three different sized chambers that have been used to study pentanol. These include the HPCC (inside diameter of 10.4 cm),[19] and Chambers I and II (inside diameters of 16.1 and 29.0 cm, respectively) described by Rudek et al. Each of these chambers have an aspect ratio of $\sim$7 or larger. The flux was calculated in each of these chambers as a function of wall heating rate (similar to the manner used to generate Fig. 5) and these results are plotted in Fig. 6 Also shown in the plot is the typical 1D prediction.

As discussed earlier, concentration-induced buoyancy can significantly reduce the flux within the chamber. Upon heating, this concentration gradient at the wall is reduced along with the convective flow that suppresses the maximum supersaturation in the center of the chamber. The flux decreases slightly with further heating, but the results are relatively insensitive to the applied heating rate.

Chamber I has an inner diameter roughly half that of Chamber II. Under identical conditions and with no applied wall heat, the model used here predicts that the concentration-induced convection is greatly reduced because of this chamber's size. In this case, the calculated flux is roughly 3 orders of magnitude lower than the 1D prediction as opposed to the 12 orders of magnitude reduction in the larger, Chamber II.

As heat is applied to Chamber I, the flux approaches the 1D value and again a plateau in the flux is reached. Although it is difficult to see in the graph, the flux does reach a maximum somewhere in the vicinity of 0.25–0.3 W cm^{-2}. Again, as heating is increased, the flux will approach the ideal heating flux value, but will entually drop as overheating occurs. For the larger chamber, these results are much more dra-

matic. It should also be noted that since convection is diminished in the smaller chamber, the ideal heating flux for this case is also closer to that predicted by the 1D model.

Finally, similar results are shown for the HPCC chamber. This chamber is typically operated without any applied wall heating. Results for Chamber II have shown that a heated chamber is preferable to no wall heating since the flux is closer to the 1D model prediction with heated walls. Because of the small size of the HPCC chamber, convection (induced by either thermal or concentration-induced buoyancy), is greatly reduced and the choice of wet or dry walls is not an issue. There is virtually no difference in the flux whether the walls are heated or not. This seems to also explain why large differences in the flux are reported for larger chambers, but little or no difference is found for the HPCC.[19] The results of our work described here suggest that it is necessary to report not only the aspect ratio, but also the size of the chamber in any future nucleation investigation. Perhaps the most important outcome of our continued analyses of TDCC operation and our empirical studies utilizing the HPCC is the conclusion that the size of the cloud chamber plays a key role in determining the operational characteristics specific to any cloud chamber. In the past, the chamber aspect ratio was considered the determining constraint in chamber design. It now seems clear that the actual size of the chamber is also an important constraint. In fact, our research indicates that it is better to use smaller chambers, e.g., the HPCC, in order to minimize the possibility of buoyancy-driven convective transport and to allow the use of a 1D model description of TDCC operation.

VI. APPLICATION TO PENTANOL DATA

In the previous section it was shown that convection tends to reduce the maximum attainable supersaturation within the TDCC. This convection is generated by buoyancy forces induced either by concentration or thermal gradients at the chamber sidewall. As shown by Fig. 5, even under ideal wall heating conditions, there can be some discrepancy between the actual chamber conditions and those predicted by the 1D model. It is also clear from the figure that the ideal heating condensation flux seems to represent a best case scenario; any departures from this ideal heating profile will only decrease the flux within the chamber further. To examine how such behavior can affect actual data we now look at recent results for pentanol taken by Rudek et al.[13]

There is currently an international effort underway to develop a high quality dataset for pentanol nucleation and Rudek et al. have reported their results for this system using two different sized chambers.[13] The first chamber, Chamber I, is approximately 16 cm in diameter while the second, Chamber II, is nearly double this size.

Rudek et al. compared their TDCC pentanol data with other expansion-based studies by plotting it in the fashion shown in Fig. 6. These other pentanol studies include data by Luijten et al.[21] using an expansion wave tube, by Hrubý et al.[22] using a nucleation pulse chamber and by Strey et al.[23] using a two-piston expansion chamber. In this plot the logarithm of the ratio of the experimentally measured
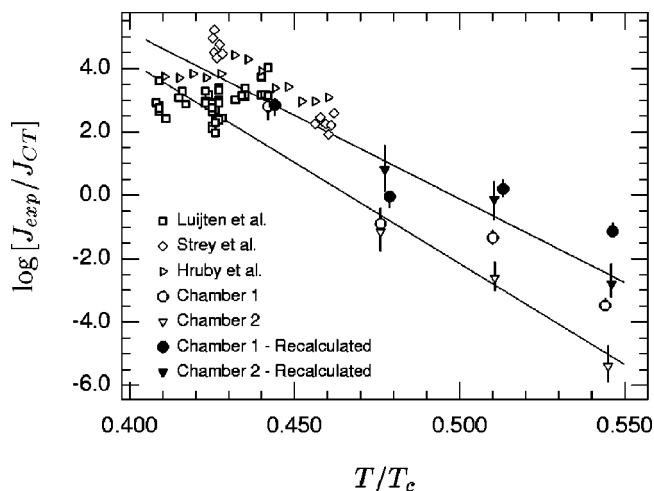
FIG. 7. Plot of the logarithm of the ratio of the experimentally measured flux to the flux calculated via CNT as a function of reduced temperature.

condensation flux to the flux calculated via CNT is plotted vs the reduced temperature.

Rudek *et al.* have fit their data from Chamber II to a line and show that the extrapolated values agree well with the expansion based studies. The data for both chambers were recalculated using the model described in this paper and the results are shown in the same plot as the filled data points. As shown in the figure, the Chamber II data are again fit to a line and a temperature-dependent correction factor is still needed to bring the experimentally measured and calculated fluxes into agreement, but the range of this correction factor has been reduced by several orders of magnitude. Further, it is expected that, because of the differences in size, the two chambers may give somewhat different results at each isotherm due to enhanced convection in the larger chamber. Although certainly not conclusive, the recalculated data points do seem to agree better and, furthermore, the extrapolated fit of the Chamber II data fits remarkably well with the lowest data point from Chamber I, as well as with the expansion studies in general.

As stated in the introduction, Anisimov also recalculated results for the pentanol data shown in Fig. 6 and found reductions at all isotherms.[12] Although we also find reductions in the supersaturation values, the reduction appears to be less dramatic than given in Ref. 12. It should also be noted that the recalculated points shown in the plot were calculated assuming ideal heating of the walls. If, in actuality, the heating was significantly different from such a profile, the supersaturation could be reduced further, resulting in a lower condensation flux. Therefore, the recalculated points shown on the graph in Fig. 6 should probably also be regarded as lower limits and may in fact be slightly higher.

VII. CONCLUSIONS

We have presented an improved model of the TDCC that includes buoyant convection and have used it to model the effect of carrier gas pressure and wall heating on the calculated chamber supersaturation. Results have shown that the calculated critical supersaturation tends to decrease with increasing pressure. This decrease occurs for both wet and dry wall operating conditions and can be relatively significant. It is likely that much of the observed pressure effect is due to this convective reduction of the supersaturation, but a quantitative comparison between the model and experimental data is needed to verify this.

A simple model of chamber wall heating was also performed and the results of this analysis were similar to what is observed experimentally. When the chamber walls are reasonably dry, the condensation flux is relatively insensitive to the amount of wall heat. With unheated walls, the flux can be several orders of magnitude lower. It was previously argued that this reduction in flux occurs because of a strong, radial diffusive concentration gradient. In actuality it occurs because of buoyant convection induced by the sidewall concentration gradient.

In general, convection tends to lower the supersaturation in the chamber over that which would be calculated via the typical 1D model of the chamber. The 1D model is, in a sense, an upper limit to the computed supersaturation profile. This reduction depends on a large number of factors (size of the chamber, amount and type of background gas, imposed temperature gradient). As of now there is no simple means to quantify this reduction. Criteria are needed to establish acceptable operating ranges for the TDCC that do not require calculations in a fully 2D model for their interpretation.

[1] R. H. Heist, M. Janjua, and J. Ahmed, J. Phys. Chem. **98**, 4443 (1994).
[2] R. H. Heist, J. Ahmed, and M. Janjua, J. Phys. Chem. **99**, 375 (1995).
[3] R. H. Heist, J. Phys. Chem. **99**, 16792 (1995).
[4] Y. Viisanen, R. Strey, and H. Reiss, J. Chem. Phys. **99**, 4680 (1993).
[5] D. W. Oxtoby and A. Laaksonen, J. Chem. Phys. **102**, 6846 (1995).
[6] I. J. Ford, *Nucleation and Atmospheric Aerosols*, edited by N. Fukuta and P. E. Wagner (Deepak, Hampton, VA, 1992), pp. 39–41.
[7] D. Kashchiev, J. Chem. Phys. **104**, 8671 (1996).
[8] K. J. Oh and X. C. Zeng, J. Chem. Phys. **114**, 2681 (2001).
[9] A. L. Itkin, Aerosol. Sci. Technol. **34**, 479 (2001).
[10] D. Kane, S. P. Fisenko, M. Rusyniak, and M. S. El-Shall, J. Chem. Phys. **111**, 8496 (1999).
[11] J. A. Fisk and J. L. Katz, J. Chem. Phys. **104**, 8649 (1996).
[12] M. P. Anisimov, S. D. Shandakov, Yu. I. Polygalov, and R. H. Heist, J. Chem. Phys. **114**, 899 (2001).
[13] M. M. Rudek, J. L. Katz, I. V. Vidensky, V. Zdimal, and J. Smolik, J. Chem. Phys. **111**, 3623 (1999).
[14] F. T. Ferguson and J. A. Nuth III, J. Chem. Phys. **111**, 8013 (1999).
[15] N. Schaeffer, F. Utheza, F. Garnier, and G. Lauriat, J. Chem. Phys. **113**, 8085 (2000).
[16] R. B. Bird, W. E. Stewart, and E. N. Lightfoot, *Transport Phenomena* (Wiley, New York, 1960).
[17] S. Patankar, *Numerical Heat Transfer and Fluid Flow* (Hemisphere, Washington, DC, 1980).
[18] A. Bertelsmann and R. H. Heist, J. Chem. Phys. **106**, 610 (1997).
[19] K. M. Colling, MS Thesis, University of Rochester (1976).
[20] Y. F. Chan, MS Thesis, University of Rochester (2001).
[21] C. C. M. Luijten, O. D. E. Baas, and M. E. H. van Dongen, J. Chem. Phys. **106**, 4152 (1997).
[22] J. Hrubý, R. Strey, and Y. Viisanen, J. Chem. Phys. **104**, 5181 (1996).
[23] R. Strey, P. E. Wagner, and T. Schmeling, J. Chem. Phys. **84**, 2325 (1986).